© 2016. Published by The Company of Biologists Ltd | Journal of Experimental Biology (2016) 219, 1146-1153 doi:10.1242/jeb.130815

RESEARCH ARTICLE

Sequential steps of macroautophagy and chaperone-mediated autophagy are involved in the irreversible process of posterior silk gland histolysis during metamorphosis of *Bombyx mori*

Hajime Shiba[1,*], Takeshi Yabu[1], Makoto Sudayama[1], Nobuhiro Mano[2], Naoto Arai[1], Teruyuki Nakanishi[3] and Kuniaki Hosono[1]

ABSTRACT

To elucidate the degradation process of the posterior silk gland during metamorphosis of the silkworm *Bombyx mori*, tissues collected on the 6th day after entering the 5th instar (V6), prior to spinning (PS), during spinning (SP) and after cocoon formation (CO) were used to analyze macroautophagy, chaperone-mediated autophagy (CMA) and the adenosine triphosphate (ATP)-dependent ubiquitin proteasome. Immediately after entering metamorphosis stage PS, the levels of ATP and phosphorylated p70S6 kinase protein decreased spontaneously and continued to decline at SP, followed by a notable restoration at CO. In contrast, phosphorylated AMP-activated protein kinase α (AMPKα) showed increases at SP and CO. Most of the Atg8 protein was converted to form II at all stages. The levels of ubiquitinated proteins were high at SP and CO, and low at PS. The proteasome activity was high at V6 and PS but low at SP and CO. In the isolated lysosome fractions, levels of Hsc70/Hsp70 protein began to increase at PS and continued to rise at SP and CO. The lysosomal cathepsin B/L activity showed a dramatic increase at CO. Our results clearly demonstrate that macroautophagy occurs before entering the metamorphosis stage and strongly suggest that the CMA pathway may play an important role in the histolysis of the posterior silk gland during metamorphosis.

KEY WORDS: Silkworm, Hsc70/Hsp70, Lysosome, Histolysis, Atg8, Cathepsin B/L, Degradation

INTRODUCTION

During insect metamorphosis, the breakdown of larval tissues is an essential process for generating raw materials to build an adult body. Histologically, the silk glands of the silkworm, *Bombyx mori*, begin to degenerate at the spinning stage and most of the tissues disappear in the early pupal stage. In the larval tissue histolysis during metamorphosis, nutrient intake and fuel levels of hemolymph are regulated by a subset of silk glands (Shimada, 1981). In addition, particular silk gland populations seem to function in the integration of fuel accessibility signals mediated by hormones such as ecdysteroids (Kamimura et al., 1997). However, the signaling pathways involved in the degradative process are poorly understood.

[1]Department of Applied Biological Science, College of Bioresource Sciences, Nihon University, 1866 Kameino, Fujisawa, Kanagawa 252-0880, Japan.
[2]Department of Marine Science and Resources, College of Bioresource Sciences, Nihon University, 1866 Kameino, Fujisawa, Kanagawa 252-0880, Japan.
[3]Department of Veterinary Medicine, College of Bioresource Sciences, Nihon University, 1866 Kameino, Fujisawa, Kanagawa 252-0880, Japan.

*Author for correspondence (chang@brs.nihon-u.ac.jp)

Received 24 August 2015; Accepted 31 January 2016

In animal cells, the target of rapamycin (TOR) signaling pathway integrates hormonal and nutrient signals to control growth and development (Sabatini et al., 1994; Schmelzle and Hall, 2000). It has been shown that increasing cellular adenosine triphosphate (ATP) levels *in vitro* increases TOR signaling, and TOR itself is thought to serve as a homeostatic ATP sensor (Dennis et al., 2001) and function as a checkpoint by which cells sense and decode changes in energy status (Jacinto and Hall, 2003).

Macroautophagy is a bulk degradation system essential for eukaryotic cell survival. It delivers cytoplasmic constituents such as aggregated proteins and organelles to the lysosome for subsequent hydrolysis (Reggiori and Klionsky, 2002). Cell signals such as starvation and other stresses are able to activate chaperone-mediated autophagy (CMA) and initiate the formation of the autophagosome, a double-membrane structure. Upon fusion with the lysosome, the sequestered contents are released into the acidic organelle from the autophagosome (Reggiori and Klionsky, 2002; Shintani and Klionsky, 2004).

In the yeast *Saccharomyces cerevisiae*, the autophagy-related genes (*ATG*s) have been identified. It has been shown that autophagosome formation requires two ubiquitin-like conjugation systems (Klionsky et al., 2003; Amar et al., 2006). In the Atg8–phosphatidylethanolamine (PE) system, Atg4, a cysteine protease, catalyzes the removal of the C-terminal arginine residue in order to uncover a glycine residue for lipidation; the glycine residue is activated and then covalently coupled to PE by Atg7, the E1-like enzyme, and Atg3, the E2-like enzyme (Ichimura et al., 2000). Consequently, Atg8 has two modified forms: an 18 kDa cytoplasmic form (form I) and a 16 kDa autophagosome membrane-associated form (form II) (Ichimura et al., 2000). In silkworm *Bombyx mori*, the autophagy-related genes (*BmATG*s) have been isolated (Zhang et al., 2009) and the expression levels of *BmATG5* and *BmATG8* in the silk gland during metamorphosis have been measured (Zhang et al., 2009). Recently, a study showed that the BmAtg8 protein contains a ubiquitin fold which is conserved in all Atg8 proteins from yeast to mammals, illustrating the importance of Atg8 protein in the macroautophagy pathway of eukaryotes (Hu et al., 2010).

Hsc70/Hsp70 participates in CMA in mammals (Chiang et al., 1989; Cuervo et al., 1997; Reggiori and Klionsky, 2002). The lysosomal proteolytic system is important for the removal of oxidized and abnormal proteins produced under stress conditions. Hsc70/Hsp70 exhibits selectivity for cytosolic substrate proteins that are degraded through this pathway (Cuervo et al., 1995, 1997, 1998, 1999, 2003). Approximately 30% of cytosolic proteins have an Hsc70/Hsp70 recognition motif, i.e. the pentapeptide KFERQ sequence (Chiang and Dice, 1988; Reggiori and Klionsky, 2002). The substrate proteins are directed to the lysosomal membrane

Journal of Experimental Biology

Journal of Experimental Biology (2016) 219, 1146-1153 doi:10.1242/jeb.130815

List of abbreviations

CMA	chaperone-mediated autophagy
CO	after cocoon formation
PS	prior to spinning
SP	during spinning
TOR	target of rapamycin
V6	6th day after entering 5th instar

through the interaction of Hsc70/Hsp70 with co-chaperones; the substrate proteins need to be unfolded in order to move into the lysosomal lumen (Agarraberes and Dice, 2001). CMA may be activated maximally upon nutritional stress although a basal level is maintained in most cells (Wing et al., 1991; Cuervo et al., 1995). In fact, the levels of Hsc70/Hsp70 in the lysosomal lumen are higher when CMA is activated during nutrient deprivation (Agarraberes et al., 1997; Chiang and Dice, 1988; Cuervo et al., 1995). CMA activity is lower in senescence cells where oxidized proteins are accumulated (Cuervo and Dice, 2000) and during renal tubular cell growth (Franch et al., 2001). Recently, there was a report showing that cytosolic Hsc70/Hsp70, the main members of the Hsp70 family, are responsible for stress responses and CMA in fish cells (Yabu et al., 2011).

It has been shown that macroautophagy plays a central role in remodeling organs in Diptera (mosquito and fruit fly; Coppens, 2011; Tracy and Baehrecke, 2013), Lepidoptera (silkworm; Goncu and Parlak, 2008; Franzetti et al., 2012; Romanelli et al., 2014) and Hymenoptera (honey bee; Silva-Zacarin et al., 2008; Santos et al., 2015). However, it is not clear whether CMA is also involved in the remodeling process. In this study, we aimed to clarify the physiological conditions and events that occur during posterior silk gland histolysis. Larval hemolymph and silk glands were collected at the following stages: the 6th day after entering the 5th instar (V6), prior to spinning (PS), during spinning (SP) and after cocoon formation (CO). Expression of the proteins Atg8 (form II), phosphorylated p70S6 kinase, phosphorylated AMP-activated protein kinase α (AMPKα), cytosolic Hsc70 and its substrate BmP109, and of ubiquitinated proteins in the posterior silk gland was analyzed; the proteins are markers of macroautophagy, TOR signaling, energy balance, CMA and the ATP-dependent ubiquitin proteasome, respectively. We also measured the concentration of ATP. Our results reveal that physiological condition changed after fasting and macroautophagy occurred before entering the metamorphosis stage. There was a dramatic increase in cytosolic Hsc70/Hsp70 and BmP109 proteins translocated into the lysosomal fraction, and lysosomal cathepsin exhibited remarkably high activity at the CO stage, suggesting the involvement of CMA in the histolysis of the posterior silk gland as well.

MATERIALS AND METHODS

Materials

Eggs of the silkworm *B. mori* (Shunrei×Shougetsu) were purchased from Ueda Sanshu (Ueda, Japan). Silkworm larvae were reared at a constant temperature of 25°C on an artificial diet (Silkmate 2S, Nihon Nosan Kogyou KK, Yokohama, Japan).

Reagents

Mouse anti-Hsc70 monoclonal antibody (SAB5200001) and mouse anti-tubulin monoclonal antibody (T6074) were purchased from Sigma-Aldrich (St Louis, MO, USA). Rabbit anti-ubiquitin polyclonal antibody (3933), mouse anti-phospho-p70S6 kinase (Thr389) monoclonal antibody (9206), rabbit anti-AMPKα polyclonal antibody (2532) and rabbit anti-phospho-AMPKα (Thr172) monoclonal antibody (2535) were obtained from Cell Signaling Technology (Boston, MA, USA). Rabbit anti-p70S6 kinase α (H-160) polyclonal antibody (sc-9027) was purchased from Santa Cruz Biotechnology (Santa Cruz, CA, USA). Rabbit anti-Atg8 polyclonal antibody (200-401-439) was purchased from Rockland (Gilbertsville, PA, USA). Alexa Fluor 594-conjugated secondary antibody (A11005) was obtained from Invitrogen (Baltimore, MD, USA). Synthetic substrates acetyl (Ac)-DEVD-4-methyl-coumaryl-7-amide (MCA; 3220-v), benzyloxycarbonyl (Z)-FR-MCA (3177-v), succinyl (Suc)-LLVY-MCA (3120-v) and 7-amino-4-methylcoumarin (AMC; 3099-v) were purchased from Peptide Institute (Osaka, Japan). Vectashield Mounting Medium with DAPI solution was purchased from Vector Laboratories (Burlingame, CA, USA).

Larval body and silk gland mass measurement

The silkworm larvae were weighed at different stages using an electronic scale (KENSEI Co. Ltd, Ibaragi, Japan), then dissected and the anterior–middle silk glands and the posterior silk glands were weighed separately.

Osmotic pressure measurement

The osmotic pressure of silkworm larvae hemolymph was measured by placing 10 µl samples into the chamber of an osmometer (5520, VAPRO® 5520 pressure osmometer, Wescor Inc., Logan, UT, USA).

Electron microscopy

Posterior silk glands were fixed with 2% paraformaldehyde and 2% glutaraldehyde in 0.1 mol l^{-1} cacodylate buffer (pH 7.4) at 4°C overnight. The silk glands were washed with cacodylate buffer three times for 30 min, then post-fixed with 2% osmium tetroxide in 0.1 mol l^{-1} cacodylate buffer (pH 7.4) at 4°C for 2 h. Dehydration of the silk glands was carried out in 50%, 70%, 90% and 100% ethanol solutions. The tissues were then infiltrated with propylene oxide two times for 30 min and immersed in a 70:30 mixture of propylene oxide and Quetol-812 resin for 1 h. After volatilization of propylene oxide overnight, the silk glands were transferred to fresh 100% Quetol-812 resin and polymerized at 60°C for 48 h. Ultra-thin sections (70 nm) generated with an ultramicrotome were mounted on copper grids and stained with 2% uranyl acetate at room temperature for 15 min. Secondary staining of the samples was carried out with lead stain solution at room temperature for 3 min after washing with distilled water. The grids were observed using a JEM-1400 Plus transmission electron microscope (JEOL Ltd, Tokyo, Japan).

Glucose measurement

The glucose content of silkworm larvae plasma was determined using the mutarotase–glucose oxidase method according to the manufacturer's instructions (Autokit Glucose; 439-90901, Wako Chemicals, Richmond, VA, USA).

ATP measurement

Silkworm larvae were dissected and the collected posterior silk glands were immediately frozen in liquid nitrogen and stored at −80°C until use. After being thawed, posterior silk glands were homogenized in 100 mg tissue per 1 ml of the following homogenization buffer: 20 mmol l^{-1} Tris-HCl (pH 7.4), 250 mmol l^{-1} sucrose, 1% Triton X-100 (w/v), 1× protease

Journal of Experimental Biology (2016) 219, 1146-1153 doi:10.1242/jeb.130815

inhibitor cocktail (11873580001, Roche Molecular Biochemicals, Mannheim, Germany). The lysates were centrifuged at 16,000 ***g*** for 15 min at 4°C to remove nuclei and unbroken tissue. Protein concentrations were determined using a Quant-iT™ Protein Assay Kit (Q33212, Molecular Probes-Life Technologies, OR, USA) and adjusted to 1 mg ml^{-1} with homogenization buffer. ATP levels were measured using a CellTiter-Glo® Luminescent Cell Viability Assay Kit (G7570, Promega, Madison, WI, USA), according to the manufacturer's instructions.

Preparation of S-100 and S-100 precipitate fractions

Frozen posterior silk gland thawed in 2.5 volumes of 20 mmol l^{-1} Hepes-KOH (pH 7.5), 10 mmol l^{-1} KCl, 1.5 mmol l^{-1} $MgCl_2$, 1 mmol l^{-1} EDTA, 1 mmol l^{-1} EGTA, 1 mmol l^{-1} DTT and 0.1 mmol l^{-1} PMSF was homogenized using a Dounce homogenizer with a loose pestle and centrifuged at 1000 ***g*** for 10 min at 4°C. The supernatant was then centrifuged at 100,000 ***g*** for 1 h at 4°C. The resulting supernatant (S-100 fraction) was used for enzyme assays and the precipitate (S-100 precipitate fraction) was used for detecting Atg8 protein. For western blot analysis, the silk gland was homogenized in the same buffer containing 1× protease inhibitor cocktail (04693116001, Roche Molecular Biochemicals). Protein concentrations were determined using a Quant-iT™ Protein Assay Kit.

Preparation of the lysosomal fraction

Lysosomes were isolated from the posterior silk gland using a Lysosome Enrichment (LE) Kit for Tissue and Cultured Cells (89839, Thermo Scientific, Rockford, IL, USA) according to the manufacturer's protocol. Briefly, 0.4 g of silk gland was homogenized in 1.6 ml of ice-cold LE Reagent A containing 1× protein inhibitor cocktail (04693116001, Roche Molecular Biochemicals) with 30 strokes in a Dounce homogenizer with a loose pestle. After addition of LE Reagent B containing 1× protein inhibitor, the lysate was centrifuged at 600 ***g*** for 15 min at 4°C. The supernatant obtained (2.4 ml) was then mixed with 800 µl OptiPrep Cell Separation Medium. The mixture (3.2 ml), which contained 15% OptiPrep medium, was then loaded into 17–30% OptiPrep gradient medium (7.6 ml) and centrifuged at 145,000 ***g*** for 2 h at 4°C. The top 3.5 ml were collected as the lysosomal fraction and stored at 4°C until used for western blotting.

Enzyme assays for proteasome and cathepsin B/L activities

Proteasome activity was measured using the synthetic substrate Suc-LLVY-MCA. The reaction mixture, which contained 10 mmol l^{-1} PIPES (pH 7.4), 2 mmol l^{-1} EDTA, 0.1% CHAPS, 0.5 mmol l^{-1} DTT, 10 mmol l^{-1} $CaCl_2$, 125 mmol l^{-1} Suc-LLVY-MCA and S-100 fraction (20 µg of protein), was incubated at 37°C for 1–2 h. Cathepsin B/L activity was measured using the synthetic substrate Z-FR-MCA. The reaction mixture, which contained 80 mmol l^{-1} sodium acetate (pH 5.5), 0.5 mmol l^{-1} DTT, 10 mmol l^{-1} $CaCl_2$, 125 mmol l^{-1} Z-FR-MCA and S-100 fraction (20 µg of protein), was incubated at 37°C for 30–60 min. The release of AMC was measured using a Versa Fluor Fluorometer (Bio-Rad, Hercules, CA, USA) with excitation at 360 nm and emission at 450 nm. One unit of enzyme activity was defined as the release of 1 nmol AMC h^{-1} at 37°C.

Western blotting

Protein samples from the S-100 fraction (40 µg) and lysosomal fraction were separated by SDS-PAGE (10% or 15% SDS-polyacrylamide gel) and electroblotted onto a polyvinylidene fluoride membrane according to Yabu et al. (2001). Anti-Atg8 polyclonal, anti-phospho-p70S6 kinase (Thr389), anti-phospho-AMPKα (Thr172), anti-Hsc70, anti-ubiquitin, anti-tubulin, anti-Hsp70 and anti-BmP109 (Tambunan et al., 1998) antibodies (1:1000) were used as the primary antibodies. Following the addition of the secondary antibody, signals were detected using a Chemi-Lumi One L Detection Kit (07880-70, Nacalai Tesque, Kyoto, Japan) according to the manufacturer's protocol.

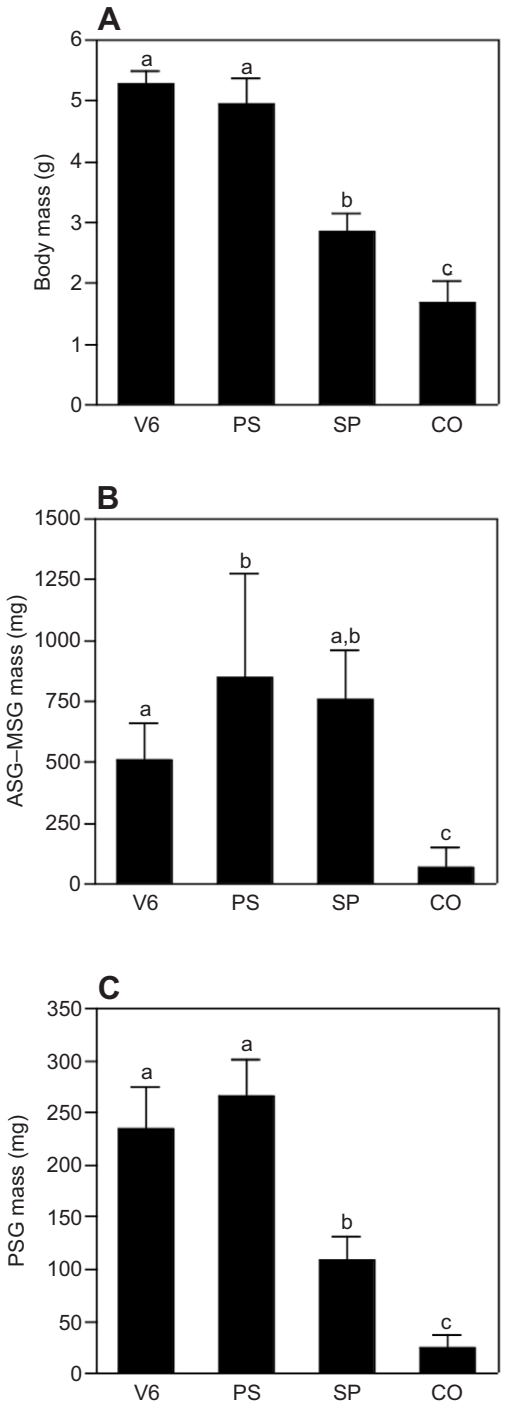

Fig. 1. Changes in body and silk gland mass during *Bombyx mori* metamorphosis. (A) Body mass. (B) Anterior–middle silk gland (ASG–MSG) mass. (C) Posterior silk gland (PSG) mass. V6, 6th day after entering 5th instar; PS, prior to spinning; SP, during spinning; CO, after cocoon formation. Each value represents the mean of 10 independent experiments; error bars represent s.d. Different letters indicate a significant difference at $P<0.05$.

Journal of Experimental Biology

Journal of Experimental Biology (2016) 219, 1146-1153 doi:10.1242/jeb.130815

Immunohistochemistry

Immunohistochemistry was performed as described previously (Yabu et al., 2008), using the following antibodies: anti-phospho-p70S6 kinase (1:100) and Alexa Fluor 594-conjugated secondary antibody (1:500) for fluorescence detection. To visualize nuclei, cross-sections of the posterior silk gland were stained with Vectashield Mounting Medium with DAPI solution. Cross-sections of posterior silk gland were made at 4 µm thickness using a cryostat (CM1850; Leica Microsystems, Tokyo, Japan). The specimens were observed under a Nikon Bi55 epifluorescence microscope (Nikon Imaging Japan Inc., Tokyo, Japan).

Statistical analysis

The results are expressed as means±s.d. Differences among groups were analyzed using one-way analysis of variance followed by Tukey's test.

RESULTS

Changes in larval body and silk gland mass

To elucidate the physiological conditions and events that occur during posterior silk gland histolysis, we first examined the mass of the larval body and silk glands at stages before (V6) and after (SP, PS and CO) entering metamorphosis. As shown in Fig. 1, a decrease in body mass occurred as the larva stopped eating at PS (wandering stage) and continued during SP and CO; the mean body mass decreased from 5.29±0.2 g at V6 to 4.95±0.4 g at PS, 2.85±0.2 g at SP and 1.69±0.3 g at CO (Fig. 1A). The total mass of the anterior and middle silk glands showed a significant increase at PS. Following a slight decrease at SP, it dropped dramatically at CO (Fig. 1B). Similar to the anterior–middle silk glands, the mass of the posterior silk gland peaked at PS. However, it showed a marked decrease at SP and CO (Fig. 1C).

Changes in osmotic pressure and glucose content of larval hemolymph

Because hemolymph is extremely important for invertebrates to maintain homeostasis and also serves as an energy source, we then investigated changes in osmotic pressure and the glucose content of larval hemolymph under histolysis conditions. As shown in Fig. 2, the changes in osmotic pressure and glucose levels in larval hemolymph were stage dependent. The osmotic pressure decreased rapidly to either the lowest level or near to it after *B. mori* entered metamorphosis stage PS (Fig. 2A). The condition was maintained at SP. A similar result was observed for glucose content. The glucose level dropped markedly at PS and continued to decrease during spinning. At CO, the level was restored to that at PS (Fig. 2B).

Occurrence of macroautophagy in the posterior silk gland

We then observed the posterior silk gland cells using a transmission electron microscope. As shown in Fig. 3, autophagosomes, which are characterized by a double membrane, and autolysosomes, which contain degraded organelles (Ylä-Anttila et al., 2009), were found in

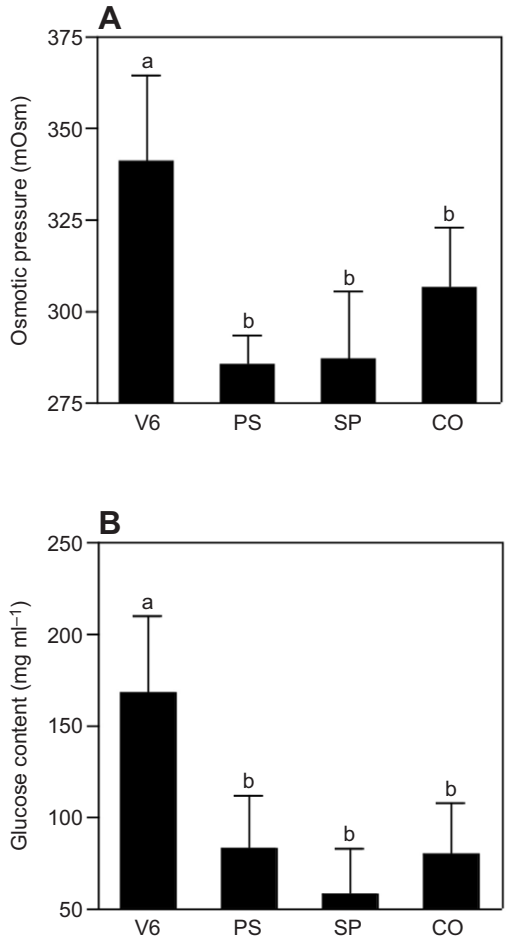

Fig. 2. Changes in osmotic pressure and glucose content of hemolymph during *Bombyx mori* metamorphosis. (A) Osmotic pressure. (B) Glucose content. V6, 6th day after entering 5th instar; PS, prior to spinning; SP, during spinning; CO, after cocoon formation. Each value represents the mean of 10 independent experiments; error bars represent s.d. Different letters indicate a significant difference at $P<0.05$.

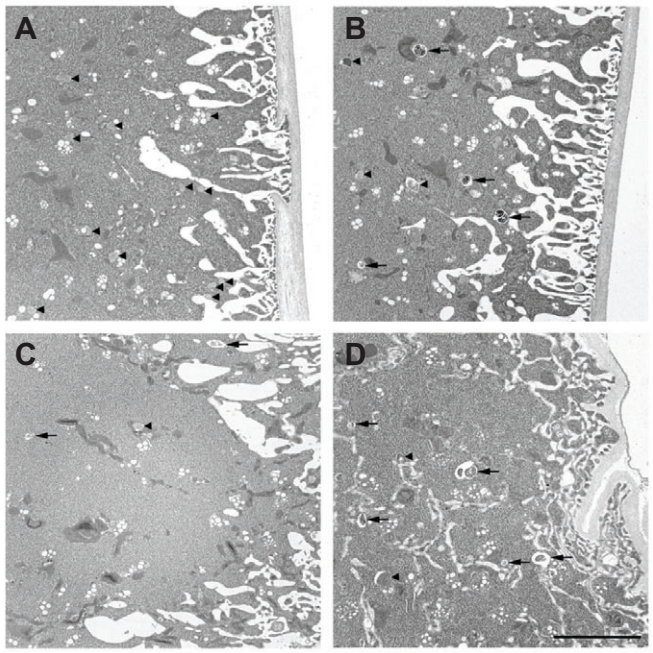

Fig. 3. Formation of autophagosomes and autolysosomes in the posterior silk gland cells during *Bombyx mori* metamorphosis. The posterior silk glands were collected at V6 (6th day after entering the 5th instar; A), PS (prior to spinning; B), SP (during spinning; C) and CO (after cocoon formation; D). Arrowheads: autophagosomes, characterized by a double membrane; arrows: autolysosomes, containing degraded organelles. Scale bar, 5 µm.

Journal of Experimental Biology (2016) 219, 1146-1153 doi:10.1242/jeb.130815

the cytoplasm at all stages. There was an increase in the number of autophagosomes/autolysosomes after entering metamorphosis at PS. Following a slight decrease at SP, the number increased again at CO.

Using a luciferase assay, we attempted to determine whether the amount of ATP in the posterior silk gland decreases rapidly after entering the metamorphosis stage, similar to the glucose content of the larval body fluid. As shown in Fig. 4A, there was a significant decrease in ATP content after entering metamorphosis stage PS. Levels continued to drop during spinning and then exhibited a significant increase after the completion of cocoon formation.

As we observed rapid decreases of glucose in the larval body fluid and ATP concentrations in the posterior silk gland after entering the metamorphosis stage, we then performed western blot analysis to examine steady-state levels of Atg8 and the phosphorylated forms of p70S6 kinase and AMPKα in the posterior silk gland. As shown in Fig. 4B, endogenous Atg8 protein, primarily form II (Atg8-II), was detected at all stages; that is, V6, PS, SP and CO. The level of phosphorylated p70S6 kinase (Thr389) was high at the feeding stage (V6) but dropped rapidly to an extremely low level at PS, during which time the larva stopped eating and entered the early metamorphosis stage; phosphorylated p70S6 kinase became undetectable at SP. Levels of total p70S6 kinase did not exhibit any fluctuation. At CO, when the larva had stopped spinning and was ready for pupation, the phosphorylated kinase increased to a level higher than that at PS. The fluctuation was parallel to that of ATP concentration. In contrast, amounts of phosphorylated AMPKα (Thr172) were high at CO and low at V6 and PS. At SP, levels were higher than at V6 and PS, but much lower than at CO. Total AMPKα was maintained at a constant level. Unlike p70S6 kinase, the increase in phosphorylated AMPKα during metamorphosis did not depend on the intracellular ATP concentration.

To examine the possible involvement of CMA in silk gland histolysis during metamorphosis, we measured steady-state levels of cytosolic Hsc70. The results show that the protein level decreased at PS and then increased at SP. The elevated levels were maintained during CO (Fig. 4B).

In addition to western blot analysis, we also carried out immunohistochemical staining of posterior silk gland cross-sections using an antibody against the phosphorylated p70S6 kinase (Thr389) protein (Fig. 4C, upper panels; nuclei stained with DAPI are shown in the bottom panels). As can be seen, the phosphorylated protein was detected in all experimental samples. In the cross-sections of the V6 and CO stages, many of the cells in the posterior silk gland, particularly the nuclear and/or perinuclear regions, showed a significant accumulation of phosphorylated p70S6 kinase proteins (Fig. 4C). In the PS and SP stages, the number of phosphorylated p70S6 kinase-positive cells decreased.

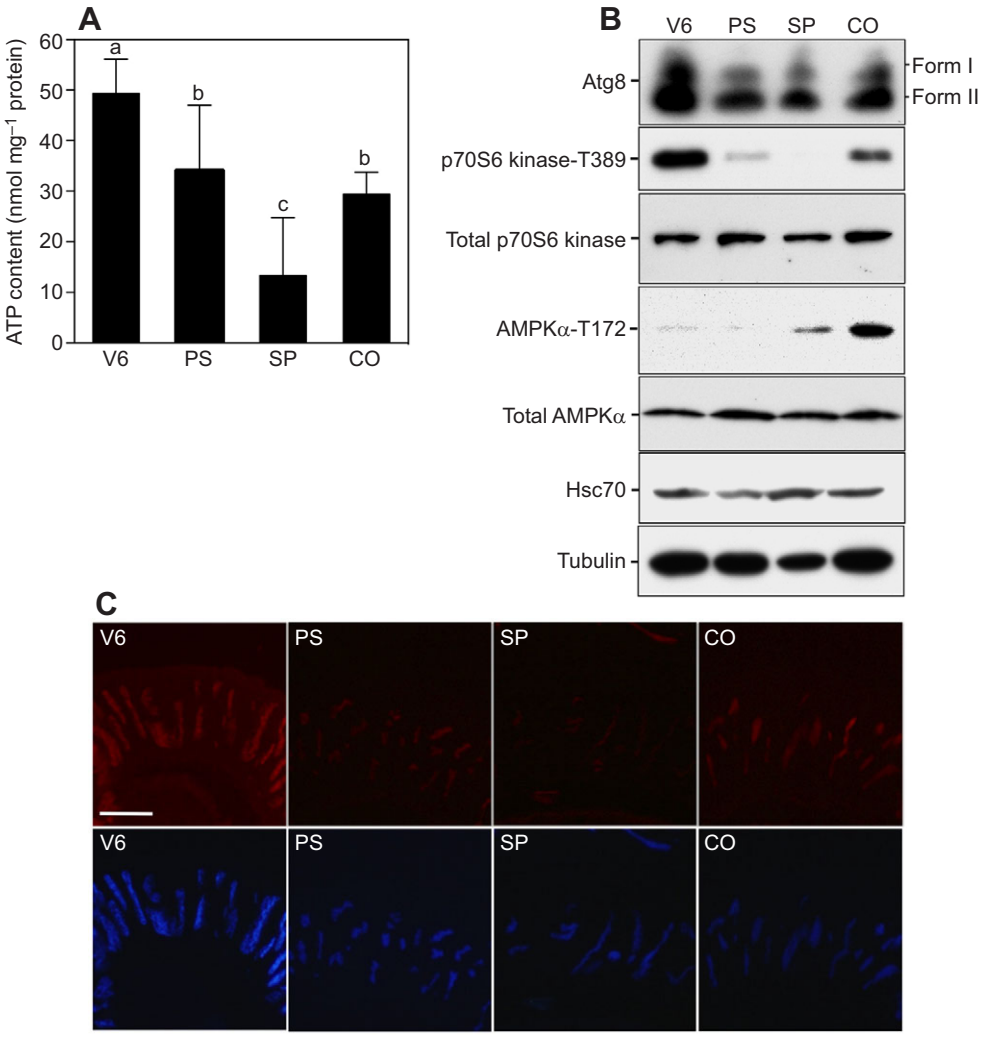

Fig. 4. Induction of macroautophagy and CMA, and suppression of TOR signaling in the posterior silk gland during *Bombyx mori* metamorphosis. The posterior silk glands were collected at V6 (6th day after entering the 5th instar), PS (prior to spinning), SP (during spinning) and CO (after cocoon formation). (A) Changes in ATP content. Each value represents the mean of six independent experiments; error bars represent s.d. Different letters indicate a significant difference at $P<0.05$. (B) Western blot analysis of total p70S6 kinase, phosphorylated p70S6 kinase (p70S6 kinase-T389), total AMPKα, phosphorylated AMPKα (AMPAα-T172), Hsc70, tubulin and Atg8. (C) Immunohistochemical analysis of the phosphorylated p70S6 kinase protein in the posterior silk gland. The cross-sections were immunolabeled with anti-phospho-p70S6 kinase antibody (upper panels) and stained with DAPI (bottom panels) to visualize nuclei. Scale bar, 50 µm. CMA, chaperone-mediated autophagy; TOR, target of rapamycin.

Journal of Experimental Biology

Journal of Experimental Biology (2016) 219, 1146-1153 doi:10.1242/jeb.130815

Examination of ATP-dependent ubiquitin-proteasome activity during metamorphosis

Besides autophagy, which is responsible for degradation of cytoplasmic organelles and long-lived proteins, the ATP-dependent ubiquitin-proteasome pathway is another system responsible for intracellular short-lived protein degradation. To investigate whether the system functions in silk gland histolysis during metamorphosis, we examined ubiquitinated protein levels using western blot analysis and proteasome activity using a synthetic substrate, Suc-LLVY-MCA. As shown in Fig. 5A, after entering the metamorphosis stage PS, there was a decrease in total ubiquitinated proteins. Levels increased more and more as metamorphosis proceeded to SP and CO. Proteasome activity was high at V6 and PS but low at SP and CO (Fig. 5B).

Localization of Hsc70/Hsp70 and BmP109 proteins in isolated lysosomes

To ensure that CMA was indeed activated during metamorphosis, we isolated lysosomes from the posterior silk gland and examined the localization of Hsc70/Hsp70 and BmP109 proteins that contained the KFERQ motif sequences (Table 1) necessary for selective degradation. Cathepsin B/L activity, the marker enzyme for lysosomes, was measured as well. As shown in Fig. 6A, the level of Hsc70/Hsp70 was low at V6. When larvae stopped eating and entered metamorphosis stage PS, it increased significantly and continued to rise during SP and CO. For the BmP109 protein, two bands were detected of molecular mass 109 and 80 kDa. Presumably, the larger band was the intact protein and the smaller band was the truncated protein. At V6, levels of intact protein were low. There was a dramatic increase after entering metamorphosis stage PS, and then a decrease at SP to levels slightly higher than those at V6; levels slightly decreased further at CO. For cathepsin B/L activity, there was a marked increase at CO (Fig. 6B), suggesting an enhancement of CMA activity at that stage.

DISCUSSION

In this study, we aimed to elucidate the physiological conditions and events that occur during posterior silk gland histolysis. As shown in Fig. 1, the larval body mass began to decrease after entering the fasting stage at PS. Larval body mass dropped quickly after a gut purge or excretion of hemolymph, which occurred between PS and SP, and then continued to decrease as the metamorphosis process proceeded. Unlike body mass, the mass of the silk gland increased even after entering the fasting or metamorphosis stage at PS, reflecting the accumulation of silk proteins in the gland. Fibroin, a silk protein, is synthesized in the posterior silk gland and then transported to the middle silk gland, where a glue protein, sericin, is synthesized (Gamo et al., 1977). It appears that the silk gland mass began to decrease between the PS and SP stages. Based on our results, it is clear that the decrease in silk gland mass at the stages chosen for this study reflect histolysis conditions well.

The levels of osmotic pressure, glucose and ATP dropped dramatically upon fasting at PS. While the levels of glucose and ATP continued to decrease at SP, osmotic pressure showed a slight increase. These results indicate that the ATP production system slows down because of a shortage of glucose in the posterior silk gland cells immediately after fasting, which in turn shifts the physiological condition to favor catabolic processes.

Western blot analysis showed that phosphorylation of p70S6 kinase decreased tremendously after fasting at PS and became undetectable at SP, while phosphorylation of AMPKα protein was markedly low at V6 and high at CO. Both TOR and AMPK are regulated by intracellular AMP/ATP ratios and function in controlling energy balance (Kahn et al., 2005). While TOR is activated under conditions of sufficient fuel and inactivated during fuel shortages, AMPK activity is increased during fuel deficiency (Kahn et al., 2005) and inhibited by nutrient signals (Minokoshi et al., 2004). Overexpression of AMPK in the hypothalamus results in increases in food intake and body mass, whereas downregulation causes constraints on food consumption (Minokoshi et al., 2004). When AMPK-dependent mechanisms are activated, they lead to the inhibition of TOR activity (Inoki et al., 2003). Our results unambiguously show that the energy balance in the posterior silk

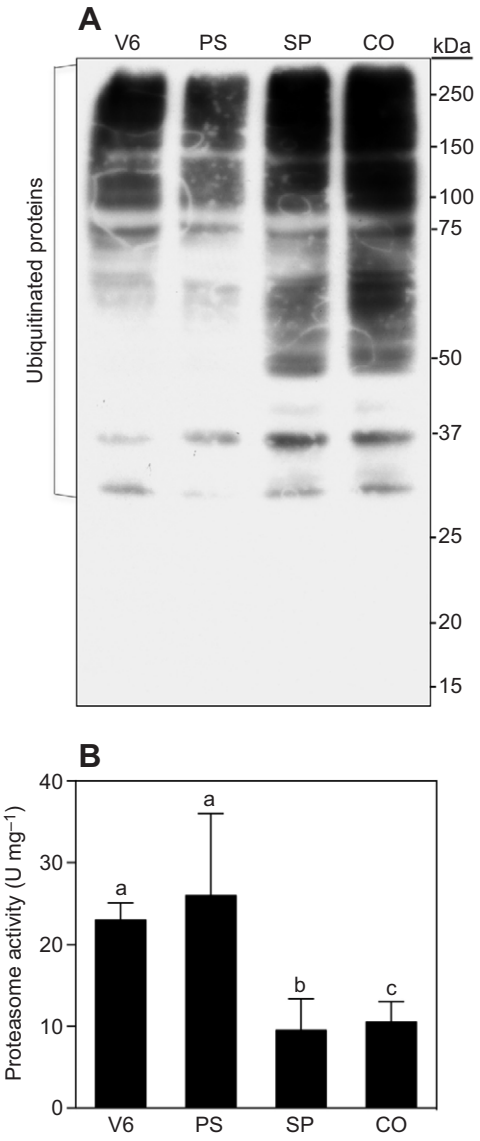

Fig. 5. Suppression of the ubiquitin-proteasome pathway in the posterior silk gland during *Bombyx mori* metamorphosis. The posterior silk glands were collected at V6 (6th day after entering the 5th instar), PS (prior to spinning), SP (during spinning) and CO (after cocoon formation). (A) Accumulation of ubiquitinated proteins. The molecular mass markers are indicated in kDa on the right. (B) Decrease in proteasome activity. Activity was measured using the S-100 fraction (20 μg protein), with Suc-LLVY-MCA as a substrate. Each value represents the mean of six independent experiments; error bars represent s.d. Different letters indicate a significant difference at $P<0.05$.

Journal of Experimental Biology

Journal of Experimental Biology (2016) 219, 1146-1153 doi:10.1242/jeb.130815

Table 1. The KFERQ-like sequences within BmP109 protein

Protein substrate	Sequence	Representation	References
BmP109 protein	QRELR	Q + – ϕ +	Tambunan et al. (1998)
	QIKDK	Q ϕ + – +	
	QFVEK	Q ϕ ϕ – +	
Hsc70 protein	QRDKV	Q + – + ϕ	Agarraberes and Dice (2001)
	QKILD	Q + ϕ ϕ –	

The listed KFERQ-like sequences found in BmP109 and Hsc70/HSP70 proteins meet the following requirement: the pentapeptide contains an acidic (D, E; representation –), a basic (K, R; representation +), a hydrophobic (V, I, L, F; representation ϕ) and either a second hydrophobic or a second basic amino acid in any order, and includes Q at the beginning or at the end (Agarraberes and Dice, 2001).

gland cells is managed in a similar way, in which TOR and AMPK act reciprocally.

By using electron microscopic observations and western blot analysis, we revealed the presence of autophagosomes and autolysosomes at all stages (Figs 3, 4B). Initially, we predicted that macroautophagy might occur after entering metamorphosis stages PS, SP and CO, based on the fact that the silkworm larva has stopped eating at these stages; macroautophagy can be induced by starvation. However, we observed that macroautophagy was already active at the V6 stage. Macroautophagy is a cellular mechanism of 'self-eating', which involves maintaining cellular homeostasis during starvation, degrading damaged cellular components and invasive pathogens (Campoy and Colombo, 2009; Lionaki et al., 2013). In addition, it plays an important role in preventing apoptosis and diseases by degrading misfolded and aggregated proteins (Bjørkøy et al., 2005; Lin and Qin, 2013; Mariño et al., 2014). Considering that V6 is the time point when fibroin is actively synthesized and the physiological condition favors anabolic processes, we speculate that macroautophagy may act in preventing aggregation of the silk protein fibroin, which has a molecular mass of 370 kDa.

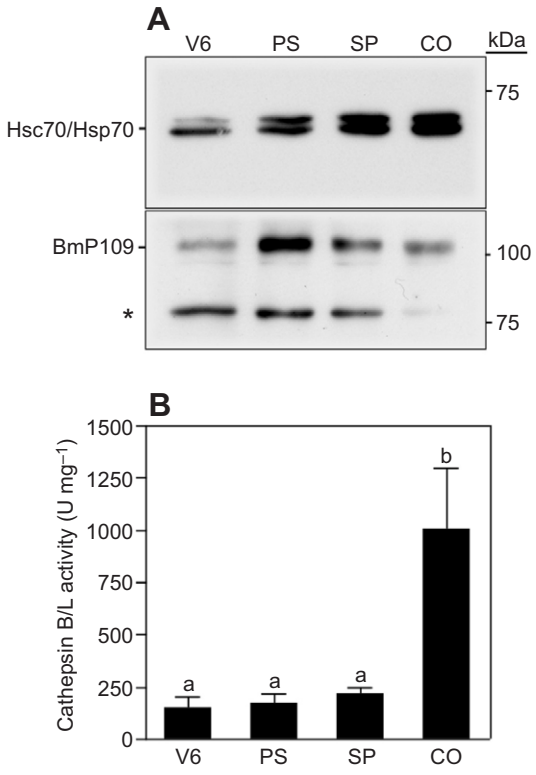

Fig. 6. Activation of chaperone-mediated autophagy in the posterior silk gland during *Bombyx mori* metamorphosis. The posterior silk glands were collected at V6 (6th day after entering the 5th instar), PS (prior to spinning), SP (during spinning) and CO (after cocoon formation). (A) Translocation of Hsc70/Hsp70 and BmP109 into the lysosome. BmP109 protein was used as a substrate for Hsc70/Hsp70. The molecular mass markers are indicated in kDa on the right. *Degradation products of BmP109. (B) Cathepsin B/L activity in the lysosomal fractions. Z-FR-MCA was used as a substrate. Each value represents the mean of six independent experiments; error bars represent s.d. Different letters indicate a significant difference at $P<0.05$.

In addition to macroautophagy, we also revealed the occurrence of CMA during silk gland histolysis. Upon entering the metamorphosis stage at PS, the level of Hsc70/Hsp70 protein in lysosomes began to increase and continued to rise during SP and CO (Fig. 6A). The enhancement of CMA activity seemed to coincide with the rapid decrease of the mass of the posterior silk gland. It has been shown that macroautophagy and CMA directly communicate with each other in protein degradation to maintain cell homeostasis (Cuervo et al., 1995; Kaushik et al., 2008). If nutritional stress continues, CMA pathway will be enhanced. Our results suggest that macroautophagy and CMA may act in a similar way to degrade the silk gland efficiently and promptly.

The levels of glucose, ATP and the phosphorylated p70S6 kinase protein showed restoration at CO. The question is why this restoration is necessary at the stage immediately before pupation. For a possible explanation, we examined the nucleus. The silk gland cells are multinucleate cells, or polykaryocytes; the nuclei are amorphous. A dramatic reduction in cell volume and shrinkage of the posterior silk gland occurs at SP and CO. Importantly, the nuclei, which cannot be removed by autophagy, remain intact in the cells; the condensed nuclei can be observed in the shrunken silk gland cross-sections of the CO stage (Kawamoto et al., 2014). Thus, the cells need to activate another degradative system to remove the nuclei and, finally, the cells themselves. In fact, we have shown that apoptotic events such as activation of BmCaspase, a homolog of caspase-3, and DNA fragmentation do occur in the shrunken silk gland after entering the pupal stage (Kawamoto et al., 2014). It seems reasonable to hypothesize that it is necessary for the cells to restore the anabolic process so that the components necessary to activate apoptosis can by synthesized to remove the remaining nuclei and the shrunken cells themselves. It has been shown that remodeling of the silkworm larval midgut occurs in a sequence in which autophagy precedes apoptosis (Franzetti et al., 2012). The results obtained from the present study reveal that the larval posterior silk gland activates the same sequence to eliminate itself.

At present, the signaling process that allows the silk gland cell to partially restore its anabolic processes at CO remains obscure and requires further clarification. The molecule that participates in this process has yet to be determined. Based on the observations that silk gland histolysis was accelerated and gene expression of BmCaspase (Kawamoto et al., 2014), an executioner of apoptosis, was induced at CO, it is quite possible that the unknown molecule may also be involved in the induction of apoptosis. To further understand this event, we are currently working to identify the pivotal molecule.

Acknowledgements
We thank Ryousuke Kawabe for providing technical assistance.

Competing interests
The authors declare no competing or financial interests.

Author contributions

H.S. and T.Y. conceived and designed the experiments. H.S., T.Y., M.S. and N.M. performed the experiments. H.S., T.Y., N.A., T.N. and K.H. analyzed the data. H.S., T.Y. and N.A. interpreted the data and wrote the manuscript.

Funding

This study was supported by an Individual Research Grant of the College of Bioresource Sciences, Nihon University.

References

Agarraberes, F. A. and Dice, J. F. (2001). A molecular chaperone complex at the lysosomal membrane is required for protein translocation. *J. Cell Sci.* **114**, 2491-2499.

Agarraberes, F. A., Terlecky, S. R. and Dice, J. F. (1997). An intralysosomal hsp70 is required for a selective pathway of lysosomal protein degradation. *J. Cell Biol.* **137**, 825-834.

Amar, N., Lustig, G., Ichimura, Y., Ohsumi, Y. and Elazar, Z. (2006). Two newly identified sites in the ubiquitin-like protein Atg8 are essential for autophagy. *EMBO Rep.* **7**, 635-642.

Bjørkøy, G., Lamark, T., Brech, A., Outzen, H., Perander, M., Øvervatn, A., Stenmark, H. and Johansen, T. (2005). P62/SQSTM1 forms protein aggregates degraded by autophagy and has a protective effect on huntingtin-induced cell death. *J. Cell Biol.* **171**, 603-614.

Campoy, E. and Colombo, M. I. (2009). Autophagy subversion by bacteria. *Curr. Top. Microbiol. Immunol.* **335**, 227-250.

Chiang, H. L. and Dice, J. F. (1988). Peptide sequences that target proteins for enhanced degradation during serum withdrawal. *J. Biol. Chem.* **263**, 6797-6805.

Chiang, H. L., Terlecky, S. R., Plant, C. P. and Dice, J. F. (1989). A role for a 70-kilodalton heat shock protein in lysosomal degradation of intracellular proteins. *Science* **246**, 382-385.

Coppens, I. (2011). Metamorphoses of malaria: the role of autophagy in parasite differentiation. *Essays Biochem.* **51**, 127-136.

Cuervo, A. M. and Dice, J. F. (2000). Age-related decline in chaperone-mediated autophagy. *J. Biol. Chem.* **275**, 31505-31513.

Cuervo, A. M., Knecht, E., Terlecky, S. R. and Dice, J. F. (1995). Activation of a selective pathway of lysosomal proteolysis in rat liver by prolonged starvation. *Am. J. Physiol.* **269**, C1200-C1208.

Cuervo, A. M., Dice, J. F. and Knecht, E. (1997). A population of rat liver lysosomes responsible for the selective uptake and degradation of cytosolic proteins. *J. Biol. Chem.* **272**, 5606-5615.

Cuervo, A. M., Hu, W., Lim, B. and Dice, J. F. (1998). IκB is a substrate for a selective pathway of lysosomal proteolysis. *Mol. Biol. Cell* **9**, 1995-2010.

Cuervo, A. M., Hildebrand, H., Bomhard, E. M. and Dice, J. F. (1999). Direct lysosomal uptake of alpha 2-microglobulin contributes to chemically induced nephropathy. *Kidney Int.* **55**, 529-545.

Cuervo, A. M., Mann, L., Bonten, E. J., d'Azzo, A. and Dice, J. F. (2003). Cathepsin A regulates chaperone-mediated autophagy through cleavage of the lysosomal receptor. *EMBO J.* **22**, 47-59.

Dennis, P. B., Jaeschke, A., Saitoh, M., Fowler, B., Kozma, S. C. and Thomas, G. (2001). Mammalian TOR: a homeostatic ATP sensor. *Science* **294**, 1102-1105.

Franch, H. A., Sooparb, S., Du, J. and Brown, N. S. (2001). A mechanism regulating proteolysis of specific proteins during renal tubular cell growth. *J. Biol. Chem.* **276**, 19126-19131.

Franzetti, E., Huang, Z.-J., Shi, Y.-X., Xie, K., Deng, X.-J., Li, J.-P., Li, Q.-R., Yang, W.-Y., Zeng, W.-N., Casartelli, M. et al. (2012). Autophagy precedes apoptosis during the remodeling of silkworm larval midgut. *Apoptosis* **17**, 305-324.

Gamo, T., Inokuchi, T. and Laufer, H. (1977). Polypeptides of fibroin and sericin secreted from the different sections of the silk gland in *Bombyx mori*. *Insect Biochem.* **7**, 285-295.

Goncu, E. and Parlak, O. (2008). Some autophagic and apoptotic features of programmed cell death in the anterior silk glands of the silkworm, *Bombyx mori*. *Autophagy* **4**, 1069-1072.

Hu, C., Zhang, X., Teng, Y.-B., Hu, H.-X. and Li, W.-F. (2010). Structure of autophagy-related protein Atg8 from the silkworm Bombyx mori. *Acta Crystallogr. Sect. F Struct. Biol. Cryst. Commun.* **66**, 787-790.

Ichimura, Y., Kirisako, T., Takao, T., Satomi, Y., Shimonishi, Y., Ishihara, N., Mizushima, N., Tanida, I., Kominami, E., Ohsumi, M. et al. (2000). A ubiquitin-like system mediates protein lipidation. *Nature* **408**, 488-492.

Inoki, K., Zhu, T. and Guan, K.-L. (2003). TSC2 mediates cellular energy response to control cell growth and survival. *Cell* **115**, 577-590.

Jacinto, E. and Hall, M. N. (2003). Tor signalling in bugs, brain and brawn. *Nat. Rev. Mol. Cell Biol.* **4**, 117-126.

Kahn, B. B., Alquier, T., Carling, D. and Hardie, D. G. (2005). AMP-activated protein kinase: ancient energy gauge provides clues to modern understanding of metabolism. *Cell Metab.* **1**, 15-25.

Kamimura, M., Tomita, S., Kiuchi, M. and Fujiwara, H. (1997). Tissue-specific and stage-specific expression of two silkworm ecdysone receptor isoforms – ecdysteroid-dependent transcription in cultured anterior silk glands. *Eur. J. Biochem.* **248**, 786-793.

Kaushik, S., Massey, A. C., Mizushima, N. and Cuervo, A. M. (2008). Constitutive activation of chaperone-mediated autophagy in cells with impaired macroautophagy. *Mol. Biol. Cell.* **19**, 2179-2192.

Kawamoto, K., Kawamoto, T., Shiba, H. and Hosono, K. (2014). A histochemical study of the posterior silk glands of *Bombyx mori* during metamorphosis from larvae to pupae using frozen sections. *Biotech. Histochem.* **89**, 145-152.

Klionsky, D. J., Cregg, J. M., Dunn, W. A., Jr, Emr, S. D., Sakai, Y., Sandoval, I. V., Sibirny, A., Subramani, S., Thumm, M., Veenhuis, M. et al. (2003). A unified nomenclature for yeast autophagy-related genes. *Dev. Cell* **5**, 539-545.

Lin, F. and Qin, Z. H. (2013). Degradation of misfolded proteins by autophagy: is it a strategy for Huntington's disease treatment? *J. Huntingtons Dis.* **2**, 149-157.

Lionaki, E., Markaki, M. and Tavernarakis, N. (2013). Autophagy and ageing: insights from invertebrate model organisms. *Ageing Res. Rew.* **12**, 413-428.

Mariño, G., Niso-Santano, M., Baehrecke, E. H. and Kroemer, G. (2014). Self-consumption: the interplay of autophagy and apoptosis. *Nat. Rev. Mol. Cell Biol.* **15**, 81-94.

Minokoshi, Y., Alquier, T., Furukawa, N., Kim, Y.-B., Lee, A., Xue, B., Mu, J., Foufelle, F., Ferré, P., Birnbaum, M. J. et al. (2004). AMP-kinase regulates food intake by responding to hormonal and nutrient signals in the hypothalamus. *Nature* **428**, 569-574.

Reggiori, F. and Klionsky, D. J. (2002). Autophagy in the eukaryotic cell. *Eukaryot. Cell* **1**, 11-21.

Romanelli, D., Casati, B., Franzetti, E. and Tettamanti, G. (2014). A molecular view of autophagy in Lepidoptera. *BioMed Res. Int.* **2014**, 1-11.

Sabatini, D. M., Erdjument-Bromage, H., Lui, M., Tempst, P. and Snyder, S. H. (1994). RAFT1: a mammalian protein that binds to FKBP12 in a rapamycin-dependent fashion and is homologous to yeast TORs. *Cell* **78**, 35-43.

Santos, D. E., Azevedo, D. O., Campos, L. A. O., Zanuncio, J. C. and Serrão, J. E. (2015). Melipona quadrifasciata (Hymenoptera: Apidae) fat body persists through metamorphosis with a few apoptotic cells and an increased autophagy. *Protoplasma* **252**, 619-627.

Schmelzle, T. and Hall, M. N. (2000). TOR, a central controller of cell growth. *Cell* **103**, 253-262.

Shimada, S. (1981). Soluble and particle-bound trehalase in the silk glands during larval-pupal development of the silkworm, Bombyx mori. *Arch. Int. Physiol. Biochim.* **89**, 341-343.

Shintani, T. and Klionsky, D. J. (2004). Autophagy in health and disease: a double-edged sword. *Science* **306**, 990-995.

Silva-Zacarin, E. C. M., Taboga, S. R. and Silva de Moraes, R. L. M. (2008). Nuclear alterations associated to programmed cell death in larval salivary glands of *Apis mellifera* (Hymenoptera: Apidae). *Micron* **39**, 117-127.

Tambunan, J., Chang, P. K., Li, H. and Natori, M. (1998). Molecular cloning of a cDNA encoding a silkworm protein that contains the conserved BH regions of Bcl-2 family proteins. *Gene* **212**, 287-293.

Tracy, K. and Baehrecke, E. H. (2013). The role of autophagy in Drosophila metamorphosis. *Curr. Top. Dev. Biol.* **103**, 101-125.

Wing, S. S., Chiang, H. L., Goldberg, A. L. and Dice, J. F. (1991). Proteins containing peptide sequences related to Lys-Phe-Glu-Arg-Gln are selectively depleted in liver and heart, but not skeletal muscle, of fasted rats. *Biochem. J.* **275**, 165-169.

Yabu, T., Kishi, S., Okazaki, T. and Yamashita, M. (2001). Characterization of zebrafish caspase-3 and induction of apoptosis through ceramide generation in fish fathead minnow tailbud cells and zebrafish embryo. *Biochem. J.* **360**, 39-47.

Yabu, T., Imamura, S., Yamashita, M. and Okazaki, T. (2008). Identification of Mg^{2+}-dependent neutral sphingomyelinase 1 as a mediator of heat stress-induced ceramide generation and apoptosis. *J. Biol. Chem.* **283**, 29971-29982.

Yabu, T., Imamura, S., Mohammed, M. S., Touhata, K., Minami, T., Terayama, M. and Yamashita, M. (2011). Differential gene expression of HSC70/HSP70 in yellowtail cells in response to chaperone-mediated autophagy. *FEBS J.* **278**, 673-685.

Ylä-Anttila, P., Vihinen, H., Jokitalo, E. and Eskelinen, E.-L. (2009). Monitoring autophagy by electron microscopy in mammalian cells. *Methods Enzymol.* **452**, 143-164.

Zhang, X., Hu, Z.-Y., Li, W.-F., Li, Q.-R., Deng, X.-J., Yang, W.-Y., Cao, Y. and Zhou, C.-Z. (2009). Systematic cloning and analysis of autophagy-related genes from the silkworm *Bombyx mori*. *BMC Mol. Biol.* **10**, 50.